In Situ Chemical Mapping of the Thin-Film Lubricated Contact

Ashley Mungroo, Denis Mazuyer, Juliette Cayer-Barrioz

▶ **To cite this version:**

Ashley Mungroo, Denis Mazuyer, Juliette Cayer-Barrioz. In Situ Chemical Mapping of the Thin-Film Lubricated Contact. Langmuir, 2024, 10.1021/acs.langmuir.4c02403 . hal-04729062

HAL Id: hal-04729062
https://hal.science/hal-04729062v1

Submitted on 9 Oct 2024

HAL is a multi-disciplinary open access archive for the deposit and dissemination of scientific research documents, whether they are published or not. The documents may come from teaching and research institutions in France or abroad, or from public or private research centers.

L'archive ouverte pluridisciplinaire **HAL**, est destinée au dépôt et à la diffusion de documents scientifiques de niveau recherche, publiés ou non, émanant des établissements d'enseignement et de recherche français ou étrangers, des laboratoires publics ou privés.

Distributed under a Creative Commons Attribution - NonCommercial - NoDerivatives 4.0 International License

LANGMUIR

Open Access
This article is licensed under CC-BY-NC-ND 4.0

pubs.acs.org/Langmuir
Article

In Situ Chemical Mapping of the Thin-Film Lubricated Contact

Ashley Mungroo, Denis Mazuyer, and Juliette Cayer-Barrioz*

Cite This: https://doi.org/10.1021/acs.langmuir.4c02403
Read Online

ACCESS | Metrics & More | Article Recommendations | Supporting Information

ABSTRACT: In this article, we propose a direct measurement of the distribution of two different chemical species in a thin-film lubricated contact under pure rolling conditions. The two chemical species were a carbonyl from an ester bond of a polyalphametacrylate (PAMA) polymer and an ether bond of a polyalphalycol (PAG) molecule, formulated in low-viscosity fluids using a mineral polyalphaolefin (PAO). A full chemical mapping of the lubricated contact region was provided thanks to the Bastet tribometer consisting of a ball-on-disk tribometer placed under a microscope coupled with an infrared spectrometer. By following the specific infrared stretching band of these two species in the inlet, contact, and cavitation areas, we showed how these molecules penetrate the high-pressure contact zone and participate in the film-formation.

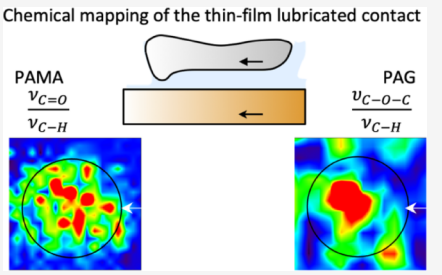

Downloaded via 92.159.154.81 on October 9, 2024 at 16:43:54 (UTC).
See https://pubs.acs.org/sharingguidelines for options on how to legitimately share published articles.

INTRODUCTION

Lubricated contacts in the elastohydrodynamic (EHD) regime display a full lubricating film that separates the two elastically deformed surfaces under a high contact pressure. Under these conditions, film formation occurs through the combination of a hydrodynamic film, contact geometry, elastic deformation, and a pressure-induced increase in fluid viscosity. The thickness of the lubricating film was first modeled by Ertel and Grubin[1] in 1945 for highly loaded contacts. They showed that the lubricant flow in the inlet governs the central film thickness, whereas the load has a weak relative impact. The Hamrock–Dowson[2] and Moes–Verner[3] predictions completed the film thickness solutions for various conditions, including piezoviscous fluids and isoviscous fluids, respectively. These predictions assume that the fluid behaves as a Newtonian fluid in the inlet zone. Most lubricants are composed of various additives, among which polymer additives are classically used as viscosity modifiers because of the ability of the polymer coils to swell with temperature and deform with shear,[4−7] and more recently as friction modifiers because of their capability to adsorb onto the surfaces.[8−12] This behavior may change the inlet flow conditions, leading to measurements of experimental film thickness diverging from the predictions.[11−15] Despite the assumption in film modeling that the fluid behaves homogeneously, the spatial distribution of the additives inside the high-pressure zone remains unknown.

In this spirit, in situ investigations of these EHD contacts have naturally begun to emerge as the micro- and nanoscale precision of the instruments has increased. Among them, spectroscopy techniques have attracted much attention for studying film composition and molecular alignment.[16,17] For instance, using Raman spectroscopy, Gardiner et al.[15] successfully matched the pressure distribution within EHD contacts with theoretical predictions. They also showed that the Petrusevich pressure spike can be qualitatively observed and located at the exit of the contact. Later, with improved measurement sensitivity and spatial resolution, Jubault et al.[17] validated the previous results by offering pressure profiles and maps describing pressure variation with load and speed under the EHD regime in pure rolling conditions. Lauer and coworkers[18−21] investigated the film temperature and demonstrated molecular alignment in the EHD contact by measuring the infrared (IR) emission. However, the sensitivity of this method was low, and the distinction between thermal and chemical information was difficult to assess. In the 90s, Cann and Spikes[22] used a Fourier transform infrared (FTIR) reflection spectroscopy to study oil-based lubricant film formation in sliding and rolling regimes within EHD contacts. To do so, an FTIR microscope was placed above a sliding point contact device between a rotating steel ball and an IR-transparent disk (diamond, sapphire, and calcium fluoride). The IR beam was focused onto the contact, reflected at the interface lubricant/ball, and then collected by the microscope detector for analysis. This approach allowed them to roughly profile the lubricant pressure through its passage in the EHD contact, following the C−H stretch wavenumber. Measurements of the central film thickness of a lubricant containing a phosphorus antiwear additive have also been reported according to the amount of reflection absorbed by the lubricating film. The main drawback of this analysis is the limited spatial resolution of 100 μm compared to the 250 μm of the contact diameter. Cann and coworkers,[17,23] also showed molecular alignment in the direction of flow of base oil, soap

Received: June 25, 2024
Revised: October 1, 2024
Accepted: October 3, 2024

© XXXX The Authors. Published by American Chemical Society

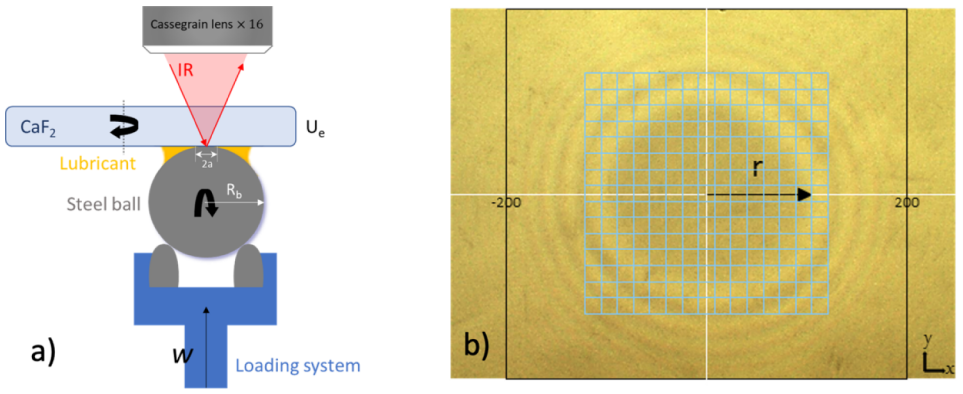

Figure 1. (a) Schematic illustration of the in situ observation of the ball-on-disk EHD contact. The entrainment speed of the ball and that of the disk is represented by the black arrows. w is the applied load whose orientation is indicated by a thin arrow. (b) Mapping region view focused on the contact area, here under w = 5.4 N with an aperture size of 15 × 15 μm^2 (blue square) in static condition. The Hertz contact zone was visible (dark circular area), and the Newton rings (succession of white/dark circles) were used to precisely locate the contact center.

grease, polymer additive, and liquid crystal molecules in the inlet and central zone of the EHD contact by employing a polarized IR signal. They also reported[24] peak intensity changes, wavenumber shifts, and band shape changes in the inlet/center/outlet of synthetic hydrocarbon base fluids. These phenomena have also been reported by Mori and coworkers for the same types of oil-based lubricants,[25] lithium and urea-based greases,[26] and water-based lubricants.[9] In the latest study, they shed light on the molecular interaction of functional groups through hydrogen bonding via shifts in peak intensities and positions, which affect the traction coefficient and film thickness.[27]

These previous studies tracing chemical species of a mineral base oil and polymers within the central zone of the contact and/or in the inlet/outlet have limitations in terms of spatial resolution, with the most precise aperture size of 25 × 25 μm^2 as reported by Hoshi,[28] and thick films, mostly in the micrometer range. Works from the literature also present trends in species distribution. In this paper, we introduced a novel approach that provides full in situ in operando chemical mapping of a submicrometric-film lubricated interface, including the inlet, high contact pressure, and outlet (cavitation) zones with an accurate resolution of 15 × 15 μm^2 over an area of 300 × 300 μm^2. This was performed by using the Bastet tribometer, and this approach was illustrated here by tracing two different chemical functions, ester and ether groups, in the thin-film EHL regime under pure rolling conditions. Fluids were formulated in low-viscosity poly-(alphaolefin) (PAO) and polyalkylene glycol (PAG). By providing a more accurate molecular mapping of the contact, we aimed at bridging the gaps presented previously by offering direct proof of the chemical group distribution prior/into/after the contact along with a qualitative evaluation. We provided clear evidence of the impact of high pressure on the molecular behavior of chemical groups in the EHD contact, and we brought fundamental insights of the film forming mechanisms.

EXPERIMENTAL SECTION

Fluids. Polyalkylmethacrylate (PAMA) polymers referred to as Viscoplex 3-200 were provided by Evonik. It is an acrylic copolymer whose molecular weight ranges between 500,000−650,000 g/mol. Oil-soluble polyalkylene glycol (PAG) Ucon OSP-32 was provided by DOW. The polyalphaolefin (PAO) base oils, PAO 8 Durasyn was provided by INEOS Oligomers and PAO40 Spectrasyn by ExxonMobil. The chemical structure of both polymers was presented in Figure SI1.

The rheological properties of the fluids were investigated using an AR 2000 from TA Instruments with a cone-plate geometry. The cone diameter was 60 mm, and the cone angle was (2°:0 min:58 s). The viscosity was measured by performing flow curves with a shear rate ranging $[10^{-2}:10^{3}]$ s^{-1} at a fixed temperature of 21 °C. Two piezoviscous fluids were formulated using two different chemical compounds. The ester lubricant PAO8-PAMA-15%w contains 15 wt % of the thickener Viscoplex 3-200 in a PAO8 base oil. The ether lubricant PAO40-PAG-50%w contains 50 wt % of PAG base oil and 50 wt % of PAO40 base oil. In the last mixture, PAG fluid has a viscosity of $\eta_0^{21°C}$ = 68 mPa·s so here, PAO40 is used as a thickener. The flow behavior of these two fluids at 21 °C gives a zero shear viscosity of $\eta_0^{21°C}$ = 0.19 Pa·s for the PAMA fluid and $\eta_0^{21°C}$ = 0.22 Pa·s for the PAG fluid. These two solutions were chosen to maintain a more or less constant low-shear viscosity.

The Bastet Tribometer: Micro-FTIR Coupled with a Tribology Tester. The Bastet tribometer shown in Figure 1a comprises two main parts: a microscope IRT-5200 coupled with an FTIR 6600 spectrometer provided by JASCO, placed above a lubricated ball-on-disk tribometer. It allows the spatial investigation of the chemistry of lubricant films under static and pure rolling conditions.

The tribometer provided by GUNT realizes a contact between an AISI52100 steel ball and a disk. The disk can rotate up to 1.8 m/s and entrain the ball in the case of a fully lubricated contact. A loading device composed of a weight cell is placed under the edge of the arm load upon which a screw is allowed to apply various loads, w, ranging from 0 to 120N ± 1N, on the ball. The steel ball radius, R_b, is equal to 12.7 mm with a Young modulus, E_b, equal to 210 GPa and a Poisson's ratio ν_b = 0.3.[29−31] The transparent disk of diameter 150 mm and thickness 4 mm ± 0.1 mm is made of calcium fluoride (CaF_2) with a Young modulus E_d = 76 GPa and a Poisson's ratio ν_d = 0.26.[29−32] The two faces of the disk are parallel and optically polished (with a surface roughness RMS of ≤ 5 nm). The choice of CaF_2 material permits the assessment of any absorbance peak in the wavenumber region ranging from 1000 to 4000 cm^{-1} thanks to the micro-FTIR spectroscopy apparatus.

The micro-FTIR device comprises a Cassegrain lens ×16 objective, allowing a maximum measurement window of 400 × 400 μm^2. It contains a mercury−cadmium−telluride (MCT) detector that allows a spectral range of 600−7800 cm^{-1} to be analyzed via the IR spectrometer. It provides a motorized aperture allowing a full sweep of the maximum observation region of 200 × 200 μm^2 for IR acquisitions. The IR mapping illustrated in Figure 1b was focused at the contact center. This will allow us to distinguish the inlet, contact zone, and outlet regions for dynamic contacts.

https://doi.org/10.1021/acs.langmuir.4c02403
Langmuir XXXX, XXX, XXX−XXX

Experimental Protocol. To analyze the lubricated contacts with the two fluids, the tribological conditions were fixed, as summarized in Table 1. Static conditions (null-velocity of both solids) as well as pure rolling (identical velocity of both solids at the contact point) conditions were investigated in this work. This choice of entrainment velocity and pressure was made to ensure elastohydrodynamic lubrication. From the mechanical and geometrical properties of the steel ball and CaF_2 disk along with these parameters, both lubricating oil films were calculated at around 300 nm, using a numerical simulation detailed in,[33] with a piezoviscous coefficient of 20 GPa^{-1} for PAO8 mixture and 22 GPa^{-1} for the formulation with PAO40. This film thickness was selected to provide a good signal-to-noise ratio and to limit the wear of the CaF_2 disk, which is unavoidable, because of the long running time of the mapping experiments.

Table 1. Tribological Conditions Fixed for the Chemical Mapping of the Two Fluids

Load, w (N)	5.4 ± 0.5
Contact radius, a (μm)	95 ± 5
Mean contact pressure (MPa)	190 ± 10
Maximum pressure, P_m (MPa)	286 ± 14
Mean entrainment speed, U_e (m/s)	0.18−0.2
Sliding over Rolling Ratio	≈0

To reduce CaF_2 disk wear, the ball was polished prior to the pure rolling experiments. After being polished, the surface roughness of the ball reached 20 nm. This value was small compared to that of the film thickness. Thus, we sought to maximize the absorbance signal under dynamic conditions by varying both the resolution and the number of scans. For PAMA and PAG fluids, the optimized protocol corresponds to a resolution of 4 cm^{-1} with 128 scans, providing sufficient running time to maximize the signal-to-noise ratio (Figure SI2). The mapping parameters were summed up in Table 2. Mappings are obtained using the areas of the absorption peaks of the considered chemical vibration or on the ratio of two different chemical vibrations.

Table 2. Mapping Parameters

Sample	PAO8-PAMA	PAO40-PAG
Aperture size	15 × 15 μm^2	20 × 20 μm^2
Mapping time	4−6 h	
Temperature	19−20 °C	
Scan number	128	
Resolution	4 cm^{-1}	

Smoothing (Gaussian type, 2D form [X = 3, Y = 3]), noise reduction (number of components = 10), and baseline correction were performed on all IR spectra to maximize the signal-to-noise ratio providing a better viewing of IR spectra. Each experiment was conducted at least twice.

RESULTS AND DISCUSSION

Homogeneous Distribution of PAMA Polymer in and Around the Static Contact. The mappings of the static contact represented in Figures 2 and 3 are based on two different chemical stretching bands. Figure 2a. is obtained by mapping the area under the characteristic peak of the C−H elongation band from 2800 to 3000 cm^{-1}. That band is found in the two chemical components present in the fluid, i.e., PAO8 and PAMA polymer, which allow us to easily identify the hertzian contact area corresponding to the absence of fluids. For such a static contact, it is possible to calculate the corresponding film thickness profile as well as the pressure profile (Figure 2b) using the Hertz theory and knowing the geometry and the mechanical properties of both solids (Table 1). In the contact center, the absence of fluids is due to the non-existence of a lubricated film. With increasing distance r from the outer edge of the hertzian contact, a homogeneous gradual increase in the area of the C−H peak is observed, which can be explained by the increase in film thickness solely driven by the geometry of the elastic deformation of the solids in static contact.

The mapping obtained from the area of the carbonyl peak of the ester groups from the PAMA polymer (Figure 3) describes a similar pattern from the previous mapping with a homogeneous increasing area of the C═O peak as the distance from the hertzian contact rises. However, the peak area of the $\nu_{C=O}$ stretching band was much lower than that in the case of the mapping of the ν_{C-H} stretching band. This reflected the high difference in the number of C−H bond present both in the PAO base oil and in the PAMA polymer backbone, compared to the carbonyl bond composing the ester group of PAMA polymer.

Heterogeneous Distribution of PAMA Polymer in the Contact Area in Pure Rolling Conditions. Mappings of the same contact based on two different chemical bondings are presented in Figure 4 by using the acquisition parameters indicated in Table 2 in pure rolling conditions.

A mapping based on the area of the absorbance peak of the ν_{C-H} stretching mode was realized, as shown in Figure 4a. The C−H band, which is characteristic of both the base oil and polymer, is present in the entire window. Therefore, this mapping provides an extensive overview of what is occurring in that area under dynamic conditions, confirming the presence of the fluid within the high-pressure zone and showing the thin-film conditions relative to the amount of fluid in the inlet. As with the mapping in static condition (Figure 2a), the dependence of the intensity of the area of ν_{C-H} peak with the distance is quite homogeneous except at the exit of the contact corresponding to the outlet zone. Another mapping was performed on the basis of the absorbance of the $\nu_{C=O}$ stretch vibration (Figure 4b). This stretching mode is characteristic of the ester groups that compose only the PAMA polymer. By comparison with the same mapping in static conditions (Figure 3), the presence of the $\nu_{C=O}$ peak in the mapping area is more heterogeneous. It reveals that the absorbance of $\nu_{C=O}$ is more important at the inlet of the contact and highlights the presence of some PAMA polymer within the contact in the high-pressure zone. In addition, the absorbance does not appear homogeneous in this zone.

A better insight into the composition of the contact was achieved by mapping the ratio $\frac{\nu_{C=O}}{\nu_{C-H}}$. As the band C═O is only present in the polymer and the band C−H is mainly present in the solvent, this ratio is qualitatively the signature of the relative presence of the polymer in the bulk composition, taking the film thickness into account. The mapping proposed in Figure 5a provided a clear evidence of the presence of PAMA polymer and its heterogeneous distribution in the contact zone: the polymer is overconcentrated in the center. This spatial distribution of polymer in the contact for such thin films was not evidenced in the literature. Using the tribological parameters of Table 1, a numerical simulation[33] was performed in order to have an insight of pressure and film thickness profiles (Figure 5b). The accumulation of PAMA polymer in the contact center matches the high pressure in the contact center. This ratio mapping also allowed the detection of the

https://doi.org/10.1021/acs.langmuir.4c02403
Langmuir XXXX, XXX, XXX−XXX

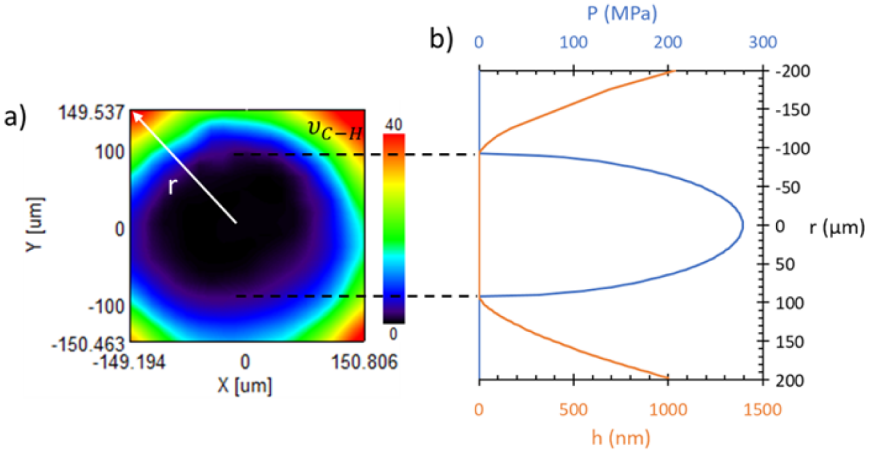

Figure 2. (a) Mapping is based on the area of the ν_{C-H} stretching band characteristic of the fluid in static conditions. The white arrow indicates the distance from the hertzian contact center. Color bar describes the intensity of the considered peak area. (b) Film thickness profile (orange) and pressure profile (blue) calculated using the experimental parameters from Table 1 in static conditions.

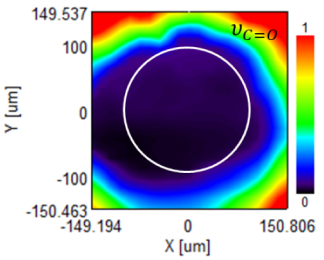

Figure 3. Mapping is based on the area of the $V_{C=O}$ stretching band specific to the ester groups composing PAMA polymer in static conditions. The white circle represents the hertzian contact obtained from Table 1. Color bar describes the intensity of the area of the considered peak.

constriction zone, where a sudden drop in the ratio signal (blue areas) was observed near the outlet zone. In the contact exit zone and on the right and left edge sides of the contact, the decrease in the relative absorbance could be associated with the horseshoe-shaped constriction zone. In the outlet, an increase in the relative absorbance is measured but is not as

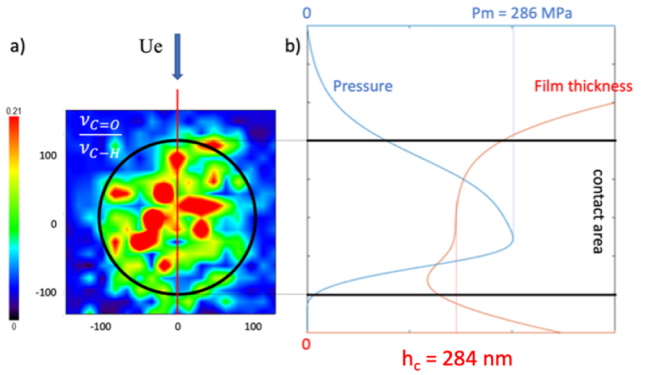

Figure 5. (a) Mapping of the contact based on the ratio of the absorption area $\frac{\nu_{C=O}}{\nu_{C-H}}$. The blue arrow illustrates the entrainment speed direction indicating the inlet zone/contact area/outlet zone from top to bottom. The circle indicates the contact diameter of 190 μm. (b) Film thickness profile (orange) and pressure profile (blue) were numerically simulated using the experimental parameters from Table 1 in pure rolling conditions.

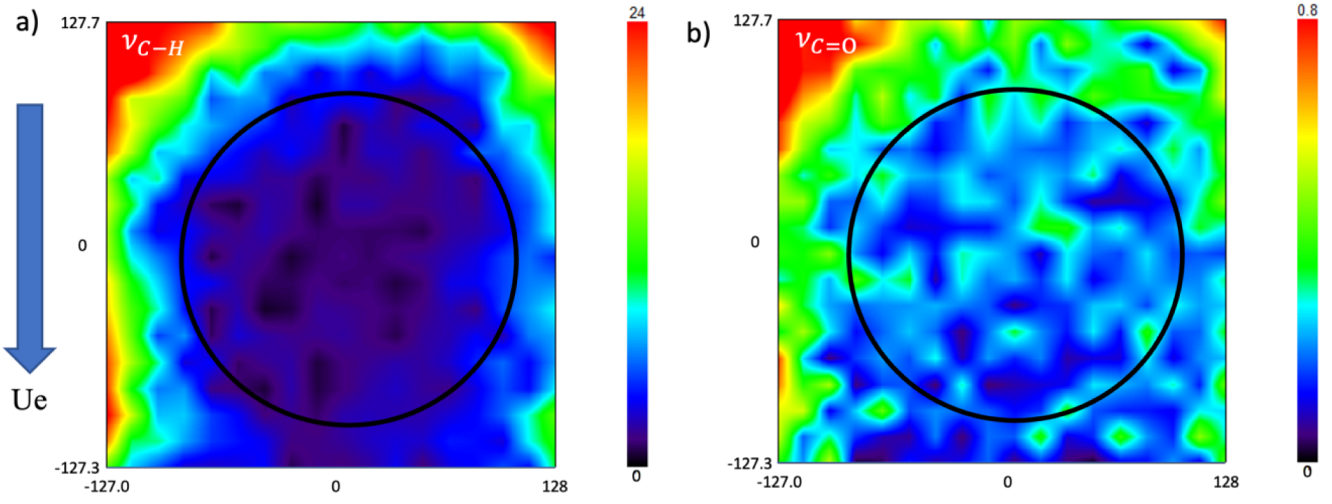

Figure 4. Mappings of the EHD contact based on the absorption area of the C−H stretch vibration (a) and the C═O stretch vibration (b). The blue arrow illustrates the entrainment speed direction: the inlet zone is on top, and the circles in the black continuous line indicate a hertzian contact diameter of 190 μm.

https://doi.org/10.1021/acs.langmuir.4c02403
Langmuir XXXX, XXX, XXX−XXX

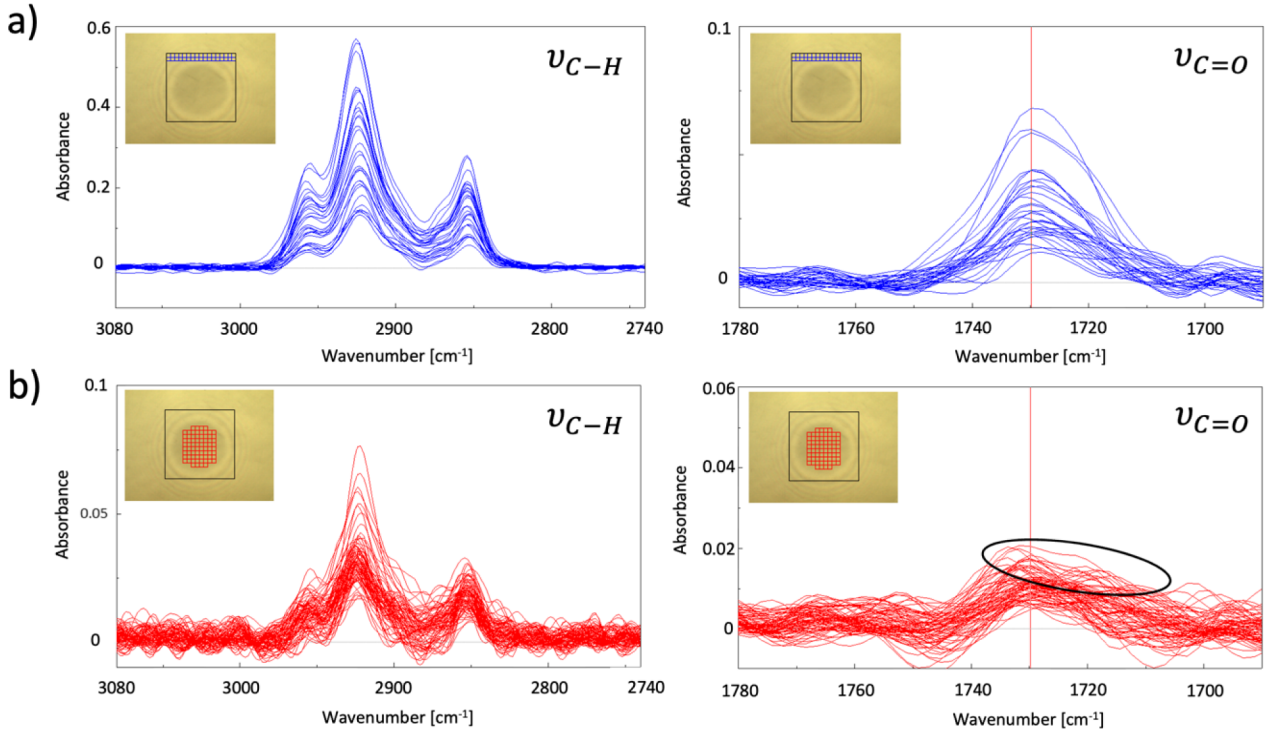

Figure 6. IR spectra of PAO8-PAMA sample at 15 wt % in the inlet (a) and the contact area (b) focused onto two chemical stretching band obtained during the mapping under the conditions described in Tables 1and2. The inset illustrates the region of the lubricated contact in which the spectra were measured from during the mapping. The vertical red line indicates le maximum of the $\nu_{C=O}$ peak at 1730 cm^{-1}. Each spectrum represents an IR spectrum performed in the aperture size 15 × 15 μm^2 represented by a small square in the contact (insert). The black circle indicates the "shoulder" effect.

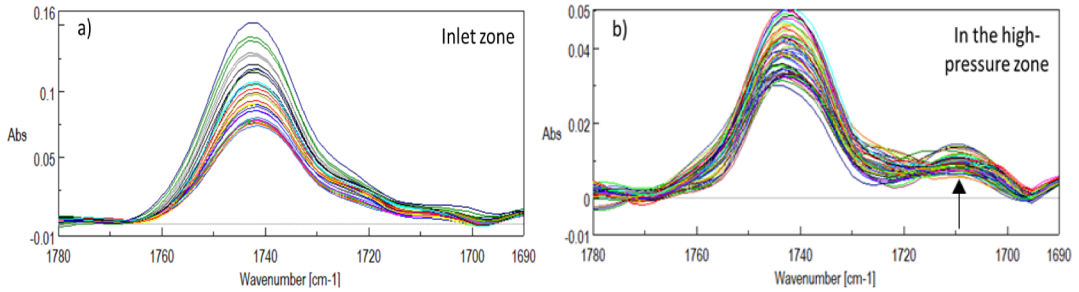

Figure 7. IR spectra of the pure ester base oil Nycobase 8318S EL in two different regions of the mapping area: (a) inlet zone and (b) center of the contact area. The red line indicates the maximum of the $\nu_{C=O}$ stretch band at 1730 cm^{-1} and the black arrow indicates the "shoulder" effect. Tribological conditions are detailed in Table 1. Each color represents an IR spectrum performed in the aperture size 15 × 15 μm^2. $w \approx 5.4$ N for U_e = 0.38 m/s.

high as in the inlet. We can conclude that the PAMA polymer tends to stay in the contact center by participating in the formation of the lubricated film due to the high pressure, which can lead to the formation of intermolecular hydrogen bonding between the carbonyl of the ester groups and hydrogens from another PAMA molecule.

A more detailed analysis of the chemical structure of the fluid film in the contact was performed by comparing the IR spectra from the inlet and contact zones for ν_{C-H} and $\nu_{C=O}$. As expected in the inlet zone (Figure 6a), the absorbance of the $\nu_{C=O}$ stretch vibration assigned to the carbonyl of the ester groups of the PAMA polymer corresponds to a well-defined peak at 1730 cm^{-1}. For both the ν_{C-H} and $\nu_{C=O}$ stretching band, a higher absorbance was measured in the inlet than in the contact center (Figure 6b). This was attributed to an increase in its concentration along with the rise of film thickness, confirming the results previously observed.[25] A modification in the form of the $\nu_{C=O}$ stretch peak was detected with the emergence of a "shoulder" effect reaching 1710 cm^{-1} as the absorbance of the main peak decreased. This spread of the peak can be explained by a change in the chemical environment surrounding the $\nu_{C=O}$ stretch vibration, which stabilizes the carbonyl, leading to a lower vibration. This could be a direct visualization of the implication of the C═O bond in hydrogen bonding on the $\nu_{C=O}$ stretch vibration.

To confirm the latter hypothesis, another contact mapping was performed for similar film thickness conditions and IR acquisition parameters but using a pure ester base oil, Nycobase 8318S EL (see Figure 7 for the normalized spectra), to promote H-bonding between the ester molecules. Because of its zero-shear viscosity is $\eta_0^{21°C}$ = 0.1 Pa·s, the entrainment speed was increased to 0.38 m/s to maintain a constant film

https://doi.org/10.1021/acs.langmuir.4c02403
Langmuir XXXX, XXX, XXX−XXX

thickness at approximately 330 nm ± 10%, according to Hamrock−Dowson prediction eq. In the inlet zone (Figure 7a), similar IR responses concerning the $\nu_{C=O}$ stretch band were observed, with the maximum absorbance at 1743 cm^{-1}. This shift of the carbonyl group from 1730 to 1743 cm^{-1} of the ester group is due to the fact that the same chemical group is observed on two different molecules, leading to two different chemical environments. Inside the hertzian contact (Figure 7b), the peak area of $\nu_{C=O}$ stretch was still present, but its amplitude was twice as low as outside the contact due to the thin film. However, the "shoulder" effect at 1710 cm^{-1} was observed and was even sharper with two well defined peaks. It clearly demonstrates that ester groups undergo intermolecular H-bonding in the contact center.[34]

It is worth mentioning that mapping was also performed using a PAMA polymer with a lower molar mass (Viscoplex 0-108). The sample was formulated at isoviscosity (C = 16.4 wt %, $\eta_0^{21\circ C}$ = 0.20 Pa·s) to keep the film thickness almost constant. This mapping did not reveal a significant increase in the absorption peak of the $\nu_{C=O}$ stretch band but rather a similar behavior in the inlet, contact, and outlet regions (Figure SI3), suggesting a weak impact of the molar mass on the entrance of the PAMA polymer within the contact, in the investigated range of molar mass. The flattening and spreading associated with the shoulder effect were also observed in the IR spectra measured into the EHD contact.

PAG Solutions, In Situ Mapping of the Ether Groups in Thin-Film Conditions. Unlike the previous formulation, the PAG molecules are to be considered as the lower viscosity component because of its weaker viscosity, whereas PAO40 acts as a thickener. The PAO40−PAG fluid mapping was based on the tracing of the ether group composing the small PAG linear chains. To achieve this, a wider aperture up to 20 × 20 μm^2 was used for a better signal-to-noise ratio. This is due to the fact that the ether group absorption peak at 1100 cm^{-1} is near the limit of the absorbance range where the CaF_2 disk starts to absorb the IR signal.[24]

Mappings of the static contact (Figure SI4) based on the u_{C-H} stretching band and ether chemical bond u_{C-O-C} stretching band allowed the hertzian contact. The mapping based on the ether bond showed a stronger absorption of the ether peak than in the case of the ester peak area mapping, allowing easier tracking of that chemical bond in the contact. Figure 8a representing IR spectra in static conditions in the inlet region exhibits a large peak associated with the u_{C-O-C} ether stretch band whose maximum absorption is at 1100 cm^{-1}.

This indicates numerous intermolecular bonds between the ether groups on a large scale. It is interesting to observe a different response of that u_{C-O-C} ether stretch band from static to dynamic conditions (Figure 8b): in the inlet zone, we observed a decomposition of the large peak into several narrow peaks with an interference-like pattern. That effect has only been observed for the u_{C-O-C} stretching band, indicating that it cannot be caused by an optical or physical effect but rather from a chemical variation. In static conditions, a broad distribution of various conformation is possible for the ether bond to be adopted allowing large intermolecular bonding. When we switched to dynamic conditions, that number of conformations was reduced leading to less intermolecular bonding. This effect was emphasized by the dynamic conditions, i.e., a high shear rate of 10^6−10^7 s^{-1}, which breaks

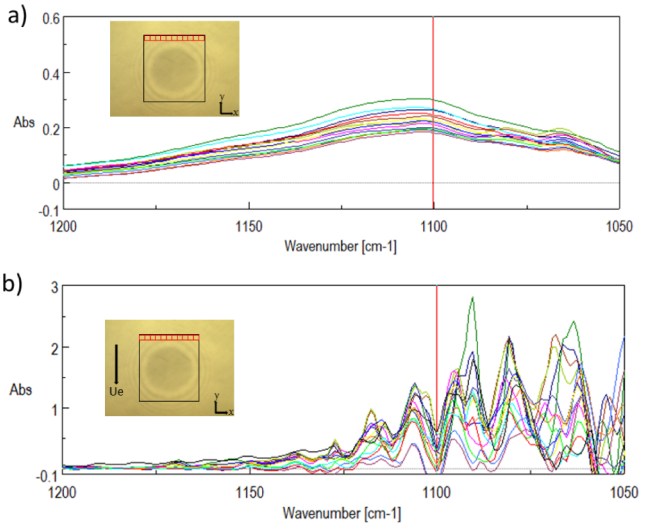

Figure 8. IR spectra of PAO40-PAG-50%w (a) in static conditions under 5.4 N at several distances from the contact center and (b) under pure rolling dynamic conditions at U_e = 0.18 m/s and w = 5.4 N. The line of red squares in the insets corresponds to the area considered for the IR spectra analysis, here 20 × 20 μm^2. Each spectrum comes from one square.

the large-scale intermolecular bonding, resulting in the apparition of multiple thinner peaks.

The IR spectra obtained in the hertzian contact illustrated in Figure 9 showed a reduction in absorbance of the u_{C-O-C} stretching band due to the weak thickness of 389 nm of the lubricated film. They also revealed that fewer conformations are allowed within the contact center, since the number of thin peaks decreased compared to IR spectra obtained in the inlet (Figure 8b) under the same conditions. This indicates that the environment of the ether groups is changed in the hertzian contact. Moreover, the appearance of a new peak at 1055 cm^{-1} corresponding to a shift of the ether band induces a stabilization of the ether bond (weaker frequency vibration), which we considered to be caused by its implication in hydrogen bonding. The mapping shown in the inset of Figure 9 is based on the absorbance area of the u_{C-O-C} ether stretch band. It indicates an inhomogeneous repartition of the PAG molecule in the contact zone compared to the mapping under static conditions (Figure SI4). We observed a higher concentration of the PAG molecule in the inlet region, similar to the observations in the case of ester groups (Figure 4b.) due to an increase in the film thickness and concentration. This is a direct proof that the accumulation of matter in the inlet region depends mainly on the dynamic properties, creating a reservoir of molecules prior to the contact region, rather than on their chemistry. This accumulation of polymer in the inlet zone can be seen as a confirmation of the overconcentration assumed by many authors in the inlet zone, to explain deviations of the film thickness evolution from the Reynolds equation solution, especially visible at low entrainment velocity by interferometry technique (see ref.[15] for instance).

The mapping based on the ratio $\frac{\nu_{C-O-C}}{\nu_{C-H}}$ in Figure 10a proves the penetration of PAG molecules in the contact center and its accumulation where the pressure is at its maximum according to the pressure profile (Figure 10b) numerically simulated using the experimental data (Table 1). In comparison with the PAO8-PAMA fluid in the same conditions at isoviscosity, this

https://doi.org/10.1021/acs.langmuir.4c02403
Langmuir XXXX, XXX, XXX−XXX

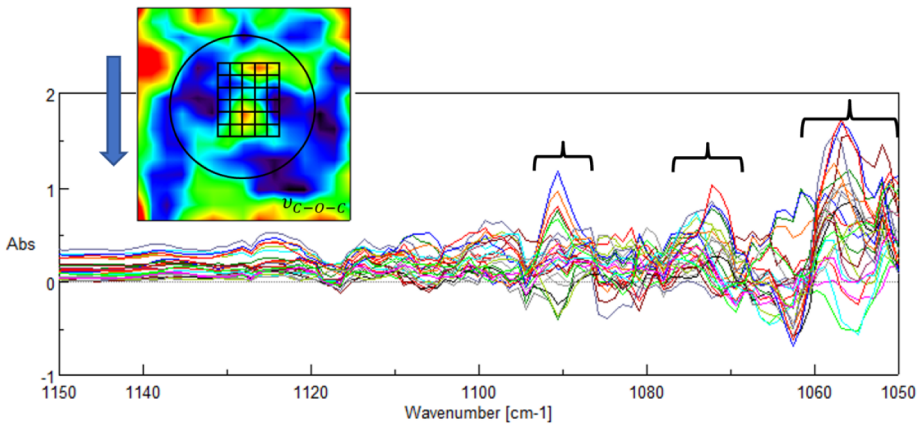

Figure 9. IR spectra obtained in the contact center during the mapping of contact zone lubricated with PAO40-PAG at 50%w at $w \approx 5.4$ N for U_e = 0.18 m/s. The main peaks discussed in the text are indicated with black hooks. The inserts represent the mapping based on the u_{C-O-C} stretching band. The black circle indicates the hertzian contact, and the black square shows the location of the considered IR spectra. The blue arrow represents the direction of the entrainment speed.

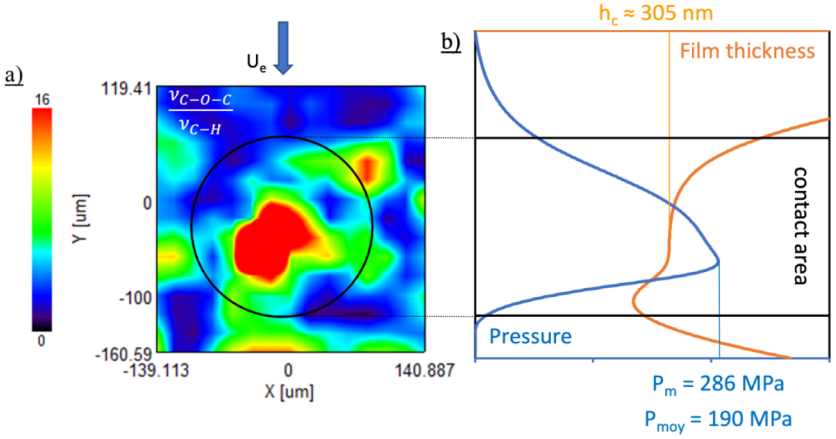

Figure 10. (a) Mapping of the contact based on the ratio of the absorption area $\frac{\nu_{C-O-C}}{\nu_{C-H}}$ of PAG lubricant at $w \approx 5.4$ N for U_e = 0.18 m/s. The blue arrow illustrates the entrainment speed direction indicating the inlet zone/contact area/outlet zone from top to bottom. The black circle indicates the contact diameter of 190 μm. (b) Film thickness profile (orange) and pressure profile (blue) numerically simulated[33] using experimental parameters from Table 1 as input, in pure rolling conditions. In that case, the central lubricant film thickness is numerically estimated to be 305 nm.

mapping revealed a greater amplitude scaling of that ratio, suggesting that PAG molecules are more likely to accumulate in the hertzian contact. This can be explained by the high difference in concentration where the ester sample contains 15 wt % of PAMA and the ether sample 50 wt % of PAG molecules, implying an easier penetration of the lower viscosity component, i.e., PAG fluid, in the contact.

By comparing the shape of the IR spectra in the contact (Figure 9) and in the inlet (Figure 8b) with the pressure profile numerically simulated in the observation window (Figure 10b), we concluded that the reduction of the decomposition of the ether band is mainly driven by the increase of the pressure, from 0.1 to 190 MPa for the mean pressure in the contact, which decreases the number of conformation allowed for the ether bond which ultimately enhances intermolecular hydrogen bonding.

CONCLUSIONS

In this work, full chemical mapping of a lubricated EHD contact was performed for pure rolling and thin film interfaces, allowing the tracking of the presence of two different chemical groups, ester and ether groups, using the Bastet tribometer under in situ and in operando conditions. This novel approach brought new fundamental insights into the film formation mechanisms. We demonstrated the entrance of the PAMA polymer and PAG molecules into the thin-film EHD contact center as well as the direct observation of the accumulation of these two polymers in the inlet and contact region under pure rolling conditions. This behavior in the inlet zone could finely explain the experimentally measured deviation from the Reynolds equation solution at low entrainment velocity with viscosity-modifier-additive solutions. We also provided strong evidence of hydrogen bonding for the PAMA polymer by the emergence of a shoulder on the carbonyl bond absorption band. Concerning PAG molecules, a shift to lower wavenumbers along with a decrease in ether bond mobility was the key feature in EHD film formation. For the PAG fluids, we also showed that the large u_{C-O-C} stretching absorption peak of the ether bond was sensitive to the high shear/pressure provided by dynamic conditions, displaying splitting peaks.

With this new analytical method, a new field of perspective opens up toward live-tracking additives within thin lubricating oil or water films and a better understanding of environmentally friendly aqueous lubricants.

https://doi.org/10.1021/acs.langmuir.4c02403
Langmuir XXXX, XXX, XXX−XXX

■ ASSOCIATED CONTENT

Supporting Information

The Supporting Information is available free of charge at https://pubs.acs.org/doi/10.1021/acs.langmuir.4c02403.

Additional experimental details, materials, and methods, including chemical structure of the molecules, IR spectra, and static contact mapping (PDF)

■ AUTHOR INFORMATION

Corresponding Author

Juliette Cayer-Barrioz − *Laboratoire de Tribologie et Dynamique des Systèmes, CNRS UMR 5513, Ecole centrale de Lyon, Ecully Cedex 69134, France;* orcid.org/0000-0002-3601-2957; Email: Juliette.cayer-barrioz@ec-lyon.fr

Authors

Ashley Mungroo − *Laboratoire de Tribologie et Dynamique des Systèmes, CNRS UMR 5513, Ecole centrale de Lyon, Ecully Cedex 69134, France*

Denis Mazuyer − *Ecole centrale de Lyon, Ecully Cedex 69134, France; Laboratoire de Tribologie et Dynamique des Systèmes, CNRS UMR 5513, Ecole centrale de Lyon, Ecully Cedex 69134, France; Institut universitaire de France (IUF), Paris 75005, France;* orcid.org/0000-0001-9828-6884

Complete contact information is available at: https://pubs.acs.org/10.1021/acs.langmuir.4c02403

Author Contributions

The manuscript was written through contributions of all authors. All authors have given approval to the final version of the manuscript. All authors contributed equally.

Notes

The authors declare no competing financial interest.

■ ACKNOWLEDGMENTS

The authors thank the TotalEnergies members Maria Rappo, Nicolas Bord, and Hélène Rodeschini for financial support of this project, and also, Arnaud Riss, Olivier Serve, and Eliette Pinel for their helpful scientific discussions. The Bastet tribometer was funded by the ADEME, the French Agency for the ecological transition via the IMOTEP project.

■ REFERENCES

(1) Grubin, A. N. *Fundamentals of the Hydrodynamic Theory of Lubrication of Heavily Loaded Cylindrical Surfaces*; Central Scientific Institute for Technology and Mechanical Engineering: Moscow, 1949.

(2) Hamrock, B. J.; Dowson, D. Isothermal elastohydrodynamic lubrication of point contacts. *J. Lubr. Technol.* **1977**, *99* (1), 15−23.

(3) Moes, H. *Lubrication and Beyond*; Twente University Press: Enschede, 2000.

(4) Barnes, H. A.*A Handbook of Elementary Rheology*; University of Wales, Institute of Non-Newtonian Fluid Mechanics, Aberystwyth, 2000.

(5) de Gennes, P. G. *Scaling Concepts in Polymer Physics*; Cornell University Press, Ithaca and London, 1979.

(6) Stachowiak, G. W.; Batchelor, A. W. *Engineering Tribology*; Butterworth-Heinemann, 2014.

(7) Rudin, A.; Schreiber, H. P. Shear modification of polymers. *Polym. Eng. Sci.* **1983**, *23* (8), 422−430.

(8) Minami, I. Molecular science of lubricant additives. *Appl. Sci* **2017**, *7* (5), 445.

(9) Mori, S. In Situ Observation of Lubricating Films by Micro-FTIR; In *Advanced Analytical Methods in Tribology*; Dienwiebel, M.; De Barros Bouchet, M.-I., Springer, 2018. DOI: .

(10) Fry, B. M.; Moody, G.; Spikes, H. A.; Wong, J. S. S. Adsorption of Organic Friction Modifier Additives. *Langmuir* **2020**, *36* (5), 1147−1155.

(11) Gmür, T. A.; Mandal, J.; Cayer-Barrioz, J.; Spencer, N. D. Towards a Polymer-Brush-Based Friction Modifier for Oil. *Tribol. Lett.* **2021**, *69* (4), 1−11.

(12) Delamarre, S.; Gmür, T.; Spencer, N. D.; Cayer-Barrioz, J. Polymeric Friction Modifiers: Influence of Anchoring Chemistry on Their Adsorption and Effectiveness. *Langmuir* **2022**, *38* (37), 11451−11458.

(13) Spikes, H. A. The behaviour of lubricants in contacts: current understanding and future possibilities. *J. Eng. Tribol.* **1994**, *208* (1), 3−15.

(14) Yahiaoui, M.; Mazuyer, D.; Cayer-Barrioz, J. Transient effects of squeeze and starvation in an EHL contact under forced oscillation: On the film-forming capability. *Tribol. Int.* **2020**, *150*, 106375.

(15) Asada, K.; Cayer-Barrioz, J.; Mazuyer, D. Elastohydrodynamic Film Formation and Sol/Gel Transition of Aqueous Fluids. *Tribol. Lett.* **2022**, *70* (4), 1−10.

(16) Albahrani, S. M. B.; Philippon, D.; Vergne, P.; Bluet, J. M. A review of in situ methodologies for studying elastohydrodynamic lubrication. *Proc. Inst. Mech. Eng., Part J* **2016**, *230* (1), 86−110.

(17) Jubault, I.; Mansot, J. L.; Vergne, P.; Mazuyer, D. In-situ Pressure Measurements Using Raman Microspectroscopy in a Rolling Elastohydrodynamic Contact. *Trans ASME* **2002**, *124*, 114−120.

(18) Lauer, J. L.; Peterkin, M. E. Traction and lubricant film temperature as related to the glass transition temperature and solidification. *ASLE Trans.* **1978**, *21* (3), 250−256.

(19) Lauer, J. L. Study of Polyphenyl Ether Fluid (5P4E) in Operating Elastohydrodynamic Contacts By Infrared Emission Spectroscopy. *J. Lubr. Technol.* **1979**, *101* (1), 67−73.

(20) Lauer, J. L.; Keller, L. E.; Choi, F. H.; King, V. W. Alignment of fluid molecules in an EHD contact. *ASLE Trans.* **1982**, *25* (3), 329−336.

(21) King, V. W.; Lauer, J. L. Temperature gradients through EHD films and molecular alignment evidenced by infrared spectroscopy. *J. Lubr. Technol.* **1981**, *103* (1), 65−73.

(22) Cann, P. M.; Spikes, H. A. In lubro studies of lubricants in EHD contacts using FTIR absorption spectroscopy. *Tribol. Trans.* **1991**, *34* (2), 248−256.

(23) Cann, P. M.; Aderin, M.; Johnston, G. J.; Spikes, H. A. An Investigation into the Orientation of Lubricant Molecules in EHD Contacts. *Tribol. Ser.* **1992**, *21* (C), 209−218.

(24) Cann, P. M.; Spikes, H. A. In-contact IR spectroscopy of hydrocarbon lubricants. *Tribol. Lett.* **2005**, *19* (4), 289−297.

(25) Goto, R.; Onodera, K.; Sato, T.; Hoshi, Y.; Nanao, H.; Mori, S. In situ FTIR observation of the polymer FM enrichment at the EHL contact. *Tribol. Online* **2020**, *15* (3), 136−141.

(26) Takahashi, K.; Shitara, Y.; Mori, S. Direct Observation of Thermo-Reversible Gel-Lubricants in EHL by FT-IR Micro-Spectroscopy. *Tribol. Online* **2008**, *3* (2), 131−136.

(27) Takiwatari, K.; Sato, S.; Hoshi, Y.; Nanao, H.; Mori, S. Effect of Functional Groups of Polyglycol Oils on Their Lubrication Properties. *Tribol. Online* **2021**, *16* (1), 24−30.

(28) Hoshi, Y.; Minami, I.; Mori, S. Change in Concentration of Water Glycol Hydraulic Fluid Near EHL Contact Region: Observation by Micro FT-IR. *Jpn. J. Tribol.* **2004**, *49* (6), 599−610.

(29) Tanaka, S.; Nakahara, T.; Kyogoku, K. Measurements of two-dimensional distribution of refrigerant concentration in EHL film using micro FT-IR and effect of variation of concentration on oil film thickness. *Tribol. Lett.* **2003**, *14* (1), 9−15.

(30) De Vicente, J.; Stokes, J. R.; Spikes, H. A. Lubrication properties of non-adsorbing polymer solutions in soft elastohydrodynamic (EHD) contacts. *Tribol. Int.* **2005**, *38* (5), 515−526.

(31) Ernesto, A.; Mazuyer, D.; Cayer-Barrioz, J. The combined role of soot aggregation and surface effect on the friction of a lubricated contact. *Tribol. Lett.* **2014**, *55* (2), 329−341.
(32) Liu, M.; Jung, S.; Kim, H.; Lee, Y. Experimental and analytical investigation into boiling induced thermal stress: Its impact on the stress state of oxide scales of nuclear components. *Nucl. Eng. Des.* **2019**, *341*, 66−72.
(33) Touche, T.; Woloszynski, T.; Podsiadlo, P.; Stachowiak, G. W.; Cayer-Barrioz, J.; Mazuyer, D. Numerical Simulations of Groove Topography Effects on Film Thickness and Friction in EHL Regime. *Tribol. Lett.* **2017**, *65* (3), 113.
(34) Takiwatari, K.; Nanao, H.; Mori, S. Effect of high pressure on molecular interaction between oleic acid and base oils at elasthydrodynamic lubrication contact. *Lubr. Sci.* **2010**, *22* (3), 89−101.

https://doi.org/10.1021/acs.langmuir.4c02403
Langmuir XXXX, XXX, XXX−XXX